Article

Fluorescence Resonance Energy Transfer Properties and Auger Recombination Suppression in Supraparticles Self-Assembled from Colloidal Quantum Dots

Xinhua Tian [1,2,†] , Hao Chang [1,†] , Hongxing Dong [1,3,4,*] , Chi Zhang [3,5,*] and Long Zhang [1,2,3,4,*]

1   Key Laboratory of Materials for High-Power Laser, Shanghai Institute of Optics and Fine Mechanics, Chinese Academy of Sciences, Shanghai 201800, China
2   School of Physical and Technology, ShanghaiTech University, Shanghai 201210, China
3   School of Physics and Optoelectronic Engineering, Hangzhou Institute for Advanced Study, University of Chinese Academy of Sciences, Hangzhou 310024, China
4   CAS Center for Excellence in Ultra-Intense Laser Science, Shanghai 201800, China
5   Department of Mechanical and Aerospace Engineering, University of Missouri, Columbia, MO 65211, USA
*   Correspondence: hongxingd@siom.ac.cn (H.D.); chizhang@ucas.ac.cn (C.Z.); lzhang@siom.ac.cn (L.Z.)
†   These authors contributed equally to this work.

Abstract: Colloid quantum dots (CQDs) are recognized as an ideal material for applications in next-generation optoelectronic devices, owing to their unique structures, outstanding optical properties, and low-cost preparation processes. However, monodisperse CQDs cannot meet the requirements of stability and collective properties for device applications. Therefore, it is urgent to build stable 3D multiparticle systems with collective physical and optical properties, which is still a great challenge for nanoscience. Herein, we developed a modified microemulsion template method to synthesize quantum dot supraparticles (QD-SPs) with regular shapes and a high packing density, which is an excellent research platform for ultrafast optical properties of composite systems. The redshift of the steady-state fluorescence spectra of QD-SPs compared to CQD solutions indicates that fluorescence resonance energy transfer (FRET) occurred between the CQDs. Moreover, we investigated the dynamic processes of energy transfer in QD-SPs by time-resolved ultrafast fluorescence spectroscopy. The dynamic redshift and lifetime changes of the spectra further verified the existence of rapid energy transfer between CQDs with different exciton energies. In addition, compared with CQD solutions, the steady-state fluorescence lifetime of SPs increased and the fluorescence intensity decreased slowly with increasing temperature, which indicates that the SP structure suppressed the Auger recombination of CQDs. Our results provide a practical approach to enhance the coupling and luminescence stability of CQDs, which may enable new physical phenomena and improve the performance of optoelectronic devices.

Keywords: colloidal quantum dots; supraparticles; auger recombination; fluorescence resonance energy transfer

1. Introduction

Colloid quantum dots are widely studied light-emitting materials with unique structures and excellent optoelectronic properties such as a wide excitation spectrum, narrow emission spectrum, good color purity, and high photoluminescence quantum yield [1–6], which make them ideal building blocks for optoelectronic devices with collective characteristics. Their emission spectrum can be tuned across the entire visible wavelength band by simply adjusting their size and type, which is attractive for applications in displays [7,8], light-emitting diodes [9–11], solar cells [12,13], and lasers [14–17]. However, the stability and collective properties required for device applications cannot be achieved by monodisperse CQDs. To build a research platform for complex multiparticle systems with collective properties and to promote the development of CQD devices with novel optoelectronic

properties, researchers often use self-assembly methods to create CQD superstructures with coupling effects [18–24]. Such superstructures are expected to exhibit new physical and optical collective properties due to the coupling between CQDs and have attracted considerable attention, and have great application prospects in catalysis [25,26], photonic materials [27], solar cells [28], and drug delivery [29]. Therefore, clarifying the superstructure construction mechanism of self-assembled CQDs and their unique collective optical properties is of great significance for the development of next generation optoelectronic devices [30–39].

In recent years, researchers have devoted tremendous efforts to the study of the optical properties of superstructured systems [40]. The microemulsion method is commonly used to control the self-assembly of a large number of CQDs into three-dimensional superstructures with spherical shapes, known as supraparticles. Previous studies on the preparation of CQD superstructures by the microemulsion method mainly focused on the relationship between experimental parameters and the final products, including the influence of the concentration of CQDs and the type of surfactant on the surface tension and stability of microemulsion droplets, as well as the control of the final morphology of the SPs by changing the volatilization conditions [41–44]. Another main direction is clarifying the mechanism of superstructure assembly by monitoring the dynamical properties of supraparticle nucleation in the process of CQD assembly [45–49]. The success of the synthesis method has enabled the use of CQDs as building blocks for multifunctional SPs. For instance, the combination of red-, green-, and blue-emitting QDs into a single SP enables white-light generation [50,51]. Additionally, the formation of micrometer-scale spherical SPs effectively combines the QDs into microcavities that support whispering gallery modes to achieve SP lasers [52–56]. However, the collective luminescence properties and spectral dynamics of quantum dot supraparticles are rarely studied [57,58]. Therefore, it is urgent and necessary to clarify the ultrafast optical processes in QD-SPs.

In this work, we synthesized spherical quantum dot supraparticles with a regular shape and high packing density using the microemulsion template method. This self-assembled SP structure enabled energy transfer between CQDs through fluorescence resonance energy transfer, resulting in a redshift in the steady-state fluorescence spectra of the SPs. Moreover, we investigated the dynamics of the energy transfer process of individual SPs by time-resolved fluorescence spectroscopy. The fast FRET process promotes rapid energy transfer between excitons, which then released energy by emitting photons. This resulted in significantly lower energy dissipation in the form of thermal energy due to Auger recombination and potentially improved stability at high temperatures. In addition, we achieved SPs with smaller particle spacing by short-chain ligand exchange, as evidenced by the faster spectral redshift rate and the faster FRET rate. Therefore, SP structures with short-chain ligands can better suppress Auger recombination, leading to better temperature stability of the SPs. Our results show that the CQD self-assembled supraparticle structure is an ideal platform for the research of multiparticle systems, and its novel FRET effect and temperature-insensitive fluorescence emission characteristics could promote the development of new types of optoelectronic devices.

2. Self-Assembly of CQDs into Supraparticles

Figure 1 shows a schematic of the synthesis of self-assembled supraparticles using CQDs as building blocks. The surface of the CQDs was passivated by long-chain organic ligands such as oleic acid and oleylamine, which spatially stabilized the colloid and limited the interaction between individual CQDs. The fabrication of self-assembled SPs from dispersed CQDs was achieved by evaporating the non-polar phases of the oil-in-water emulsions. Nearly monodisperse droplets of the CQD solution (oil phase) were formed using microfluidic chips, and specific size droplets could be prepared by accurately controlling the shear force and relative flow rate of the oil and water phases. These formed droplets were dispersed in an aqueous phase containing surfactants, which imparted spatial stability to the droplets and prevented them from fusing or breaking. The CQDs were

confined to the microemulsion drop by the hydrophobic interaction between the surface ligand and the surfactant. After the formation of the microemulsions, the CQDs began to assemble with the evaporation of the low-boiling solvent in the droplet. The concentration of CQDs increased with the evaporation process, and as the volume fraction of CQDs increased to 20%, the CQDs began to aggregate through hydrophobic interactions [46]. Evaporation time is related to droplet size, oil phase type, and many other factors affecting the evaporation rate. After the oil phase evaporated completely, solid SPs were formed, which were bound together by van der Waals forces and no longer dispersed in polar or non-polar solvents [45,59]. The slow evaporation rate of the oil phase resulted in the formation of SPs with a regular spherical structure and smoother surface. These SPs were stabilized in the aqueous phase through the hydrophobic interaction of surfactants, and their optical properties did not change significantly even after being stored in water for months. By combining the microemulsion method with microfluidics, we can precisely control the size of the SPs by adjusting the size of microemulsion droplets and the initial concentration of CQDs in the oil phase.
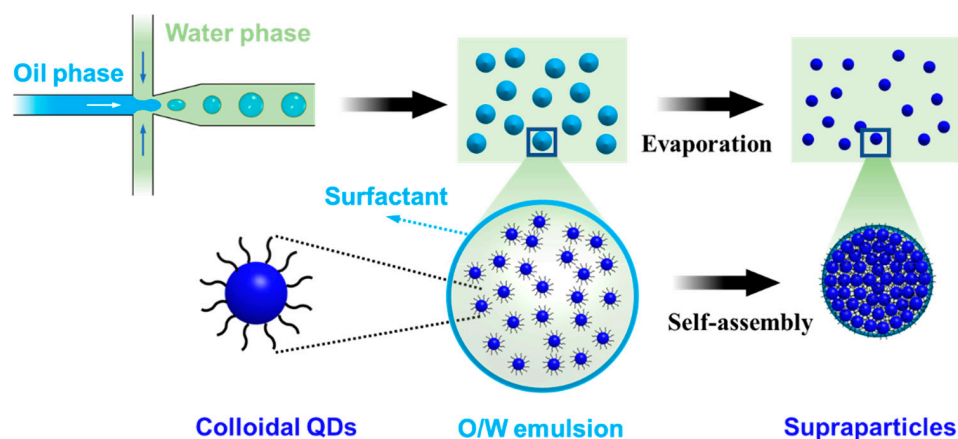

Figure 1. Schematic of the fabrication of colloidal quantum dot supraparticles through the microemulsion method.

3. Structural Characterizations of Supraparticles

The surface morphology and spatial structure of the synthesized SPs were characterized by scanning electron microscopy (SEM) and transmission electron microscopy (TEM). As shown in Figure 2a, most of the SP samples were spherical with a size distribution of 1.0 ± 0.2 μm due to interfacial tension during the volatilization of the oil phase. The inset of Figure 2a presents a high-resolution image of an individual SP microsphere, illustrating its regular spherical structure and smooth surface. To further investigate the internal structure of SP microspheres, TEM analysis was performed. Figure 2b shows a high-angle annular dark field (HAADF) TEM image of an individual SP microsphere, indicating that the SP microsphere was composed of a large number of CQDs. Due to the presence of hydrophobic surface ligands, the spacing of CQDs in SPs was about 3 nm, which is less than 2 times the length of oleic acid ligands. This indicates that the cross-linking between ligands in the SPs made it difficult to redisperse in solvents, and the smooth surface of the SPs can be attributed to the high filling factor of the cross-linked long-chain ligands. In Figure 2c, the fast Fourier transform of the TEM image clearly shows that the CQDs were disordered in the SPs, forming an amorphous glassy structure as expected. Previous studies have shown that if the basic constituent particles have regular spherical shapes and the same size, and their interactions can be well approximated with a hard sphere model, the SPs will form superlattice structures with icosahedral or face-centered cubic structures [41,45,60,61]. In our experiment, the initial CQDs building blocks were irregularly spherical and polydisperse, resulting a random arrangement of CQDs in SPs rather than superlattice structures despite the high packing factor (as show in Figure S1). These SPs were tightly packed via cross-linked ligands, resulting in an interparticle spacing of 3 nm, less the twice distance

between ligand layers (Figure S1). Furthermore, as shown in Figure 2d, energy dispersive X-ray spectroscopy (EDS) confirmed the uniform distribution of CQDs in SPs. These results show that the as-prepared QD-SP samples have a regular shape, and the CQDs are tightly packed in SP microspheres without agglomeration and rupture. In addition, the SPs can be stored in water and had good solution operability, making them promising for further integration into functional materials and devices.
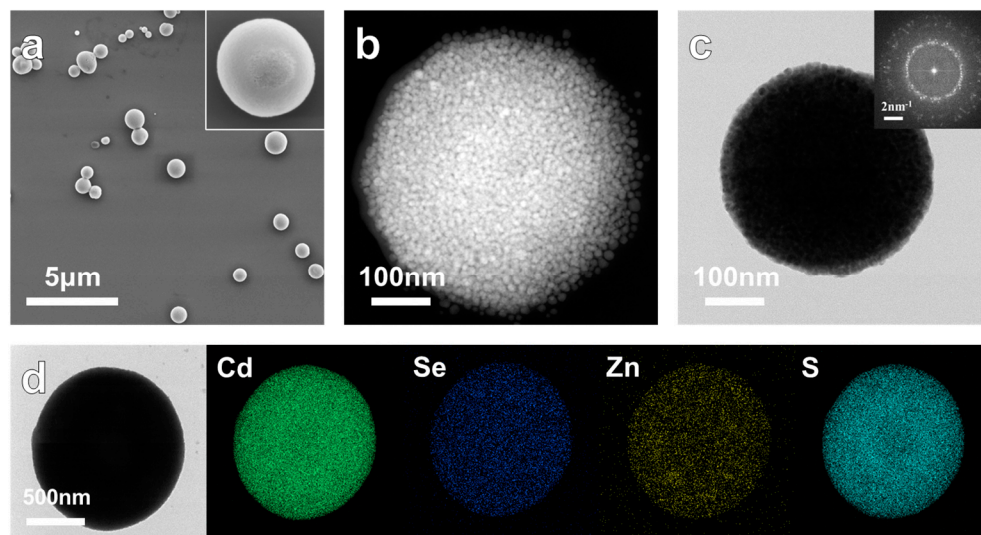

Figure 2. Structural characterization of supraparticles. (**a**) Typical SEM image of the supraparticles. Inset: magnified image of an individual supraparticle. (**b**) Representative high-angle annular dark field scanning transmission electron microscopy (HAADF-STEM) image of a supraparticle. (**c**) TEM image of a single QD-SP. Inset: the fast Fourier transform of the QD-SP. (**d**) EDS elemental mapping for cadmium, selenium, zinc, and sulfur to show the composition of the microspheres.

4. Single Supraparticle Spectroscopy and Analysis

The optical properties of the prepared QD-SP microspheres were characterized by a confocal micro-photoluminescence spectrometer. Figure 3a shows the absorption and emission spectra of dispersed CQD solution, as well as the emission spectrum of an individual SP microsphere. The photoluminescence (PL) emission center of dispersed CQD solutions was 1964 meV (631 nm) and the absorption spectrum showed the lowest exciton transition at 2025 meV (612 nm), and the emission spectrum of an individual SP was centered at 1944 meV (637 nm). We observed that the emission spectrum was slightly redshifted (20 meV) after the CQDs were assembled into SPs, which can be attributed to the fluorescence resonance energy transfer by short-range dipole–dipole coupling interactions between adjacent CQDs [62]. CQDs exhibit quantum size effects, and their size in colloidal solutions is not ideally uniform but follows a Gaussian distribution, resulting in CQDs having different exciton energies. When the distance between adjacent CQDs is less than 10 nm, small CQDs (with larger exciton energies) can act as donors while large CQDs (with smaller exciton energies) act as acceptors, activating FRET from small to large CQDs. We further investigated the energy dynamic processes of the SP samples using time-resolved and spectrum-resolved fluorescence spectroscopy to provide a more systematic demonstration of FRET. To quantify the energy transfer dynamics between CQDs, we excited the CQD solutions and SPs with 80 fs pulses (1 kHz repetition rate) using a wavelength of 400 nm. Figure 3c,d and Figure S2 show the emission intensity as a function of emission wavelength and time that was obtained using a streak camera. After exciting CQD solutions and SPs with femtosecond pulsed laser, we measured the time-resolved PL spectra on a time scale of 100 ps (Figure 3e,f). The results showed that the PL spectra of dispersed CQD solutions had a time-independent peak energy of 2037 meV. In contrast, the PL spectra of QD-SPs had an initial emission peak at 2035 meV, which

matches the emission peak of dispersed CQD solution (this spectrum reflects the actual size distribution of CQDs). However, the emission peak rapidly redshifted within the next 100 ps and stabilized at 2020 meV after more than 100 ps, indicating that the energy transfer process had stopped.
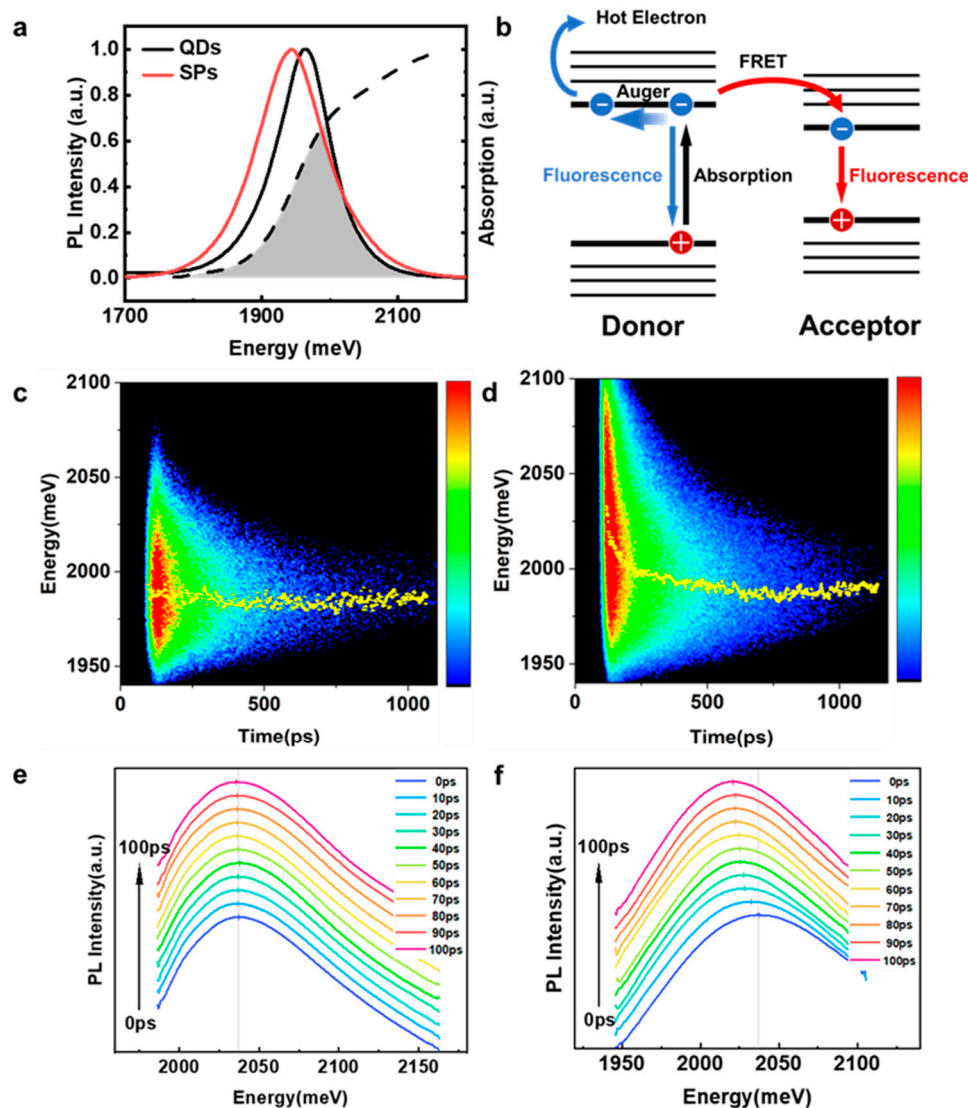

Figure 3. (**a**) Absorption (black dashed line) and emission (black curve) spectra for the CQD solution and emission spectrum for the SPs (red curve). (**b**) The excited-state pathways in a CQDs supraparticle considered in our model. (**c**,**d**) Spectrally resolved transient photoluminescence of (**c**) CdSe/ZnS CQD solution and (**d**) CQD supraparticles. (**e**,**f**) Emission spectra of CdSe/ZnS CQD solution (**e**) and CQD supraparticles (**f**) at 100 ps delay time after an excitation pulse. The short vertical bars are the peak energies. The gray vertical line is the PL peak energy of the first spectrum at 0 ps.

In order to elucidate the physical mechanism of PL spectra shift in self-assembled CQDs, we further analyzed the time-resolved PL spectra. First, we compare the transient PL decay curves of the dispersed CQD solution and a single SP at different emission wavelengths, as shown in Figure 4a,b. When the filter for wavelength selection was used, PL decay in the CQD solutions was almost wavelength-independent, which indicates that the CQDs in solution were independent emitters without any coupling or interaction between them. In contrast, PL decay at different wavelengths in SPs clearly revealed the time-dependent dynamics of FRET between CQDs. At short wavelengths, PL decayed faster at the initial stage, and the PL lifetime gradually increased with the increase in wavelength.

Furthermore, we fitted the lifetime data in Figure 4b with the bi-exponential equation $y(t) = A_0 + A_1 \exp(-t/\tau_1) + A_2 \exp(-t/\tau_2)$, where τ_1 and τ_2 represent fast and slow decay times, and A_1 and A_2 represent their contribution percentages, respectively. The fitting parameters are summarized in Table S1 and plotted in Figure 4c,d. As wavelength increased, we found that the fast decay time (52.5–64.8 ps) and slow decay time (308.6–355.4 ps) increased, but the fast component ratio decreased from 60% to 35%, while the slow component ratio increased from 40% to 65%. Since the fast and slow decay components come from non-radiative and radiative recombination processes, the fast component fraction decreased rapidly with wavelength from 595 to 620 nm, indicating that exciton energy was transferred from small to large CQDs due to dipole–dipole coupling interactions. In smaller CQDs, most excitons transferred energy to lower bandgap CQDs rather than radiative recombination. In contrast, excitons in larger CQDs received energy from FRET and radiated photons, which produced a longer PL lifetime than smaller CQDs. Data analysis of the ultra-fast time-resolved PL decay clearly showed the fast FRET process between different CQDs in SPs from high energy excitons to low energy excitons; indirect coupling via photon reabsorption was ruled out because it would not change the PL lifetime decay rate of the CQDs.
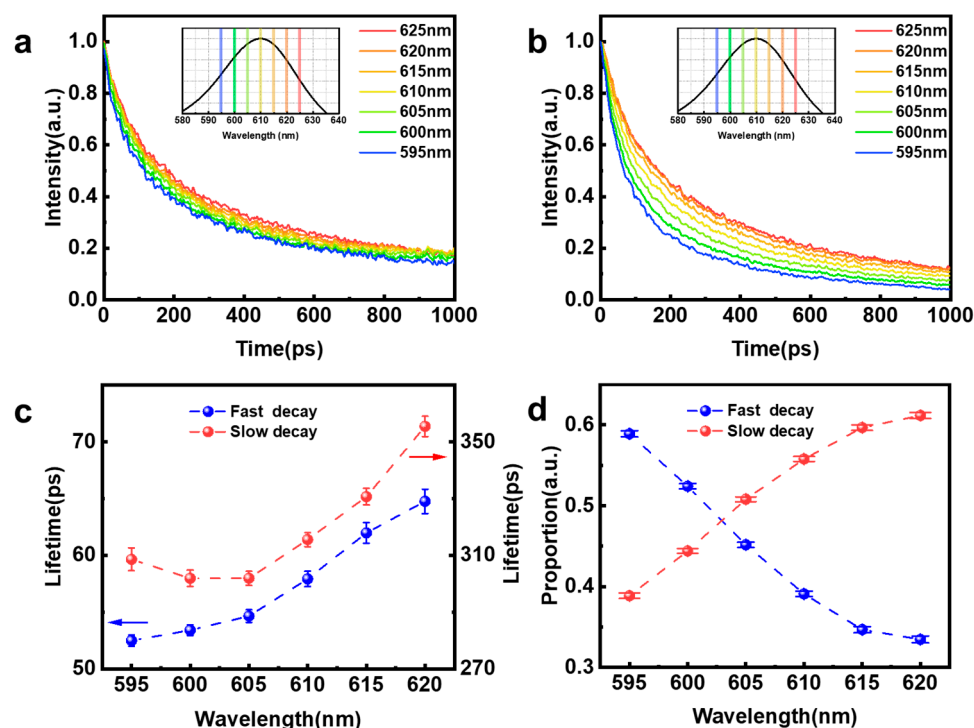

Figure 4. The energy transfer in CQD solution and QD-SPs. (**a**,**b**) Typical time-resolved photoluminescence decay curves of CQD solution (**a**) and QD-SPs (**b**) at various wavelengths. (**c**,**d**) The fast decay time and slow decay time of CQD solution (**c**) and SPs (**d**) PL decay curves with the emission peak in the range of 595 to 620 nm.

5. Suppression of Auger Recombination

The fluorescence resonance energy transfer has been demonstrated to be an effective means of enhancing the performance of sensing and light-harvesting functions [63]. In contrast to FRET, the non-radiative Auger recombination process can lead to the loss of energy in the form of heat, leading to reduced efficiency for CQD-based applications [64,65]. We noted that the FRET has an energy transfer mechanism similar to Auger recombination, but Auger recombination releases energy in the form of heat. Therefore, we suspect that when FRET occurs between CQDs, excitons transfer energy rapidly to neighboring excitons and then recombine to emit photons, reducing the probability of Auger recombination and thus inhibiting Auger recombination within CQDs. At higher excitation fluences, the

transient PL of SPs showed an increased radiation lifetime compared with the CQD solution (Figure 5a), with a slow lifetime component of 9.6 ns for the CQD solution and 12.2 ns for the QD-SPs. Moreover, temperature-dependent PL showed that the PL intensity of the CQD solution decreased more rapidly with increasing temperature than QD-SPs (Figure 5b). The QD-SP structure was better at withstanding temperature increases (Figure 5b shows a lower slope), and considering the high correlation between Auger recombination and temperature [66], this difference suggests that the QD-SP structure effectively suppressed this non-radiative recombination process. To further verify the relevance of FRET to AR, we used a short-chain Octylamine (OctA) ligand exchange strategy to replace the long-chain organic oleic acid (OA) ligand, reducing the inter-dot distances in SPs (as show in Figure S2). Considering the strong distance-sensitivity of FRET, reducing the dot spacing will improve FRET efficiency, which can be manifested by an increase in spectral redshift [62]. Figure 5c shows the PL spectra of the dispersed CQD solution, OA-SPs, and OctA-SPs at room temperature. The emission centers of the three CQD structures were 1964 meV, 1944 meV, and 1930 meV, respectively. The spectrum of OctA-SPs was redshifted by 30 meV compared to 20 meV in the spectrum of OA-SPs. In addition, the PL emission centers of the dispersed CQD solution did not change after the ligand exchange, suggesting that the short-chain ligand increased the rate of FRET. Furthermore, we measured the temperature-dependent PL spectra of the dispersed CQD solution, OA-SPs, and OctA-SPs, as shown in Figure 5d. Under the same excitation conditions, the PL intensities of the three different CQD structures decreased to 10% of the initial value when the temperature increased to 310 K, 360 K, and 400 K, respectively. These results show that the SP structure achieved the acceleration of FRET process and the suppression of Auger recombination, improving the efficiency of CQD-based devices and has a promising application prospect in carrier-multiplication-enhanced photovoltaics and electrically pumped lasers [67].
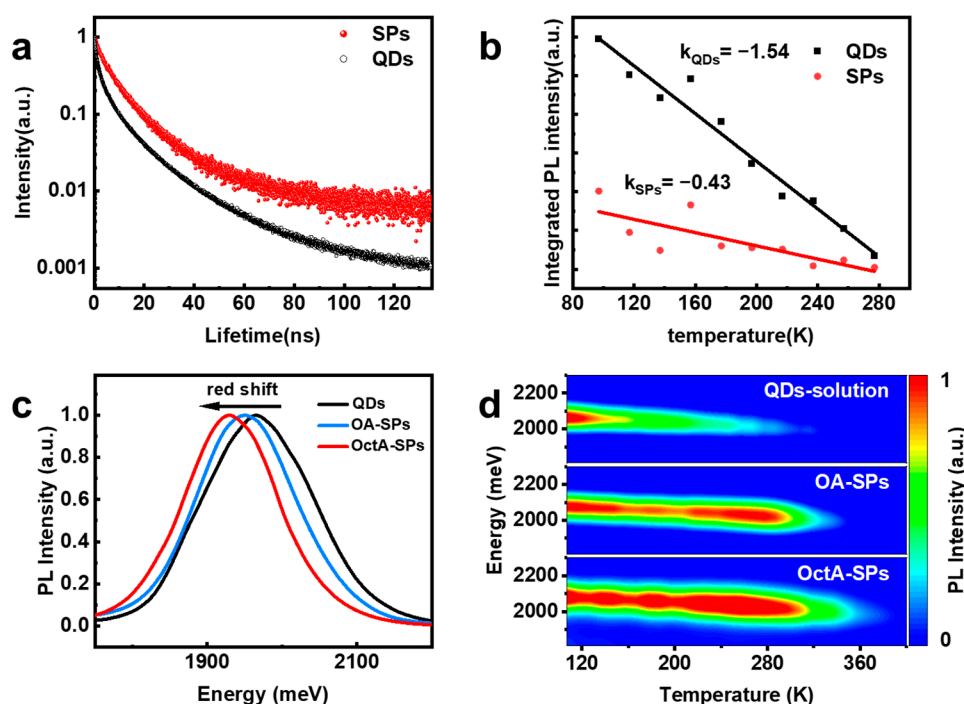

Figure 5. Auger recombination suppression using supraparticles. (**a**) PL decay of CQD solution and supraparticles. (**b**) Temperature-dependent PL intensity of CQD solution and supraparticles. (**c**) PL spectra of CQD solution, oleic acid ligand SPs, octylamine ligand SPs. (**d**) Contour plots of the temperature-dependent emission from different ligands supraparticles with the temperature varying from 110 to 400 K under the same excitation conditions.

6. Materials and Methods

6.1. Synthesis of Supraparticles Structures

Colloidal CdSe/ZnS quantum dots were obtained commercially (Xingzi (Shanghai, China) New Material Technology Development Co., Ltd.). We assembled QDs into supraparticles using an emulsion-based, bottom-up, self-assembly process following previously reported methods with slight modifications. In this work, we used microfluidic chips instead of ultrasonic methods to produce monodisperse oil-in-water microemulsion droplets. In a typical experiment, we prepared a solution of CdSe/ZnS QDs in hexane at a concentration of ~20 mg/mL as the dispersed phase and a solution of sodium dodecyl sulfate (SDS) in deionized water at a concentration of ~6 mg/mL as the continuous phase. We then connected a commercial microfluidic chip to a multichannel pressure regulator to generate monodisperse hexane microdroplets, controlling their size by adjusting the flow rates of the dispersed and continuous phases. We collected the resulting microemulsion in a glass vial covered with parafilm pierced by several 0.5 mm holes to slow down evaporation and stirred it at room temperature for 12–18 h until the hexane in the oil phase had fully evaporated. After evaporation, we washed the resulting QD SPs by three rounds of centrifugation (5000 rpm, 2 min) and redispersed them in deionized water to remove the residual surfactants. For ligand exchange of QD-SPs, we centrifuged the originally prepared SPs (5000 rpm, 2 min), added 1 wt% octylamine in 1 mL methanol, and mixed the solution at 500 rpm under magnetic stirring for 20 min. After 20 min, we washed the ligand-exchanged QD-SPs by centrifugation (5000 rpm, 2 min) and redispersed them in methanol and water to remove the residual ligands. We then drop-cast the dispersion of QD-SPs onto the desired substrate (silicon for SEM imaging and glass for spectroscopy) and dried it under a vacuum.

6.2. Structural Characterization

The SEM measurements were performed using field-emission scanning electron microscopy (FE-SEM; Auriga S40, Zeiss, Oberkochen, Germany) operated at 1 kV. The TEM measurements were performed using the Tecnai G2 F20 S-TWIN (FEI, Hillsboro, OR, USA) operated at 200 KV. The samples were prepared on a clean silicon wafer and then transferred onto a 300-mesh copper TEM grid by slightly touching the sample to the mesh.

6.3. Optical Characterization

Photoluminescence spectra were measured using a confocal microphotoluminescence system (LabRAM HR Evolution) with a high-numerical-aperture microscopy objective (N.A. = 0.5, 50×). The PL spectra were excited by a femtosecond laser (Libra, Coherent, B40 fs, 10 kHz, Santa Clara, CA, USA). Absorption spectra were measured using a PerkinElmer UV/VIS/NIR spectrometer (Lambda 750, Villeneuve-d'Ascq, France). The time-resolved PL measurements were performed using a streak camera with picosecond-order time resolution (Optronis, SC-10, Kehl, Germany). Low-temperature measurements were performed using a cryostat (80–475 K, Janis ST-500, Woburn, MA, USA) with a temperature controller (cryocon 22C, USA) and liquid N_2 for cooling.

7. Conclusions

In summary, we demonstrated a self-assembly method for preparing spherical SPs with a regular structure and smooth surface. The high packing density made the SP structure very stable in both water and air, and had good solution processability. PL spectroscopy and time-resolved experiments showed that the decay rate of PL intensity gradually increased with the increase in pump energy due to FRET, and the PL spectrum gradually redshifted with time. As the FRET rate increased, non-radiative Auger recombination of the CQDs was suppressed, and temperature-dependent PL spectra confirmed that the SP structure was more effective in suppressing Auger recombination than dispersed CQDs. Through short-chain ligand exchange, we further verified that the highly packed SPs had better high temperature optical properties, which can be attributed to the increased

FRET rate and suppressed Auger recombination in the SPs with smaller dot spacings. These properties make SP structures very attractive for applications in biosensors and light-emitting devices.

References

1. Barak, Y.; Meir, I.; Shapiro, A.; Jang, Y.; Lifshitz, E. Fundamental Properties in Colloidal Quantum Dots. *Adv. Mater.* **2018**, *30*, e1801442. [CrossRef] [PubMed]
2. Chen, O.; Zhao, J.; Chauhan, V.P.; Cui, J.; Wong, C.; Harris, D.K.; Wei, H.; Han, H.-S.; Fukumura, D.; Jain, R.K.; et al. Compact high-quality CdSe-CdS core-shell nanocrystals with narrow emission linewidths and suppressed blinking. *Nat. Mater.* **2013**, *12*, 445–451. [CrossRef] [PubMed]
3. Yin, Y.; Alivisatos, A.P. Colloidal nanocrystal synthesis and the organic-inorganic interface. *Nature* **2005**, *437*, 664–670. [CrossRef] [PubMed]
4. Liu, M.; Chen, Y.; Tan, C.-S.; Quintero-Bermudez, R.; Proppe, A.H.; Munir, R.; Tan, H.; Voznyy, O.; Scheffel, B.; Walters, G.; et al. Lattice anchoring stabilizes solution-processed semiconductors. *Nature* **2019**, *570*, 96–101. [CrossRef]
5. Cargnello, M.; Johnston-Peck, A.C.; Diroll, B.T.; Wong, E.; Datta, B.; Damodhar, D.; Doan-Nguyen, V.V.T.; Herzing, A.A.; Kagan, C.R.; Murray, C.B. Substitutional doping in nanocrystal superlattices. *Nature* **2015**, *524*, 450–453. [CrossRef]
6. Peng, X.; Lv, L.; Liu, S.; Li, J.; Lei, H.; Qin, H. Synthesis of Weakly Confined, Cube-Shaped, and Monodisperse Cadmium Chalcogenide Nanocrystals with Unexpected Photophysical Properties. *J. Am. Chem. Soc.* **2022**, *144*, 16872–16882. [CrossRef]
7. Shirasaki, Y.; Supran, G.J.; Bawendi, M.G.; Bulovic, V. Emergence of colloidal quantum-dot light-emitting technologies. *Nat. Photonics* **2013**, *7*, 13–23. [CrossRef]
8. Chang, H.; Dong, H.; Zhao, J.; Zhang, L. Efficient and stable solid state luminophores with colloidal quantum dots-based silica monolith. *Solid State Commun.* **2020**, *305*, 113765. [CrossRef]
9. Yang, Y.; Zheng, Y.; Cao, W.; Titov, A.; Hyvonen, J.; Manders, J.R.; Xue, J.; Holloway, P.H.; Qian, L. High-efficiency light-emitting devices based on quantum dots with tailored nanostructures. *Nat. Photonics* **2015**, *9*, 259–266. [CrossRef]
10. Kagan, C.R.; Lifshitz, E.; Sargent, E.H.; Talapin, D.V. Building devices from colloidal quantum dots. *Science* **2016**, *353*, aac5523. [CrossRef]
11. Zhao, B.; Yao, Y.; Gao, M.; Sun, K.; Zhang, J.; Li, W. Doped quantum dot@silica nanocomposites for white light-emitting diodes. *Nanoscale* **2015**, *7*, 17231–17236. [CrossRef] [PubMed]
12. Swarnkar, A.; Marshall, A.R.; Sanehira, E.M.; Chernomordik, B.D.; Moore, D.T.; Christians, J.A.; Chakrabarti, T.; Luther, J.M. Quantum dot-induced phase stabilization of alpha-CsPbI3 perovskite for high-efficiency photovoltaics. *Science* **2016**, *354*, 92–95. [CrossRef] [PubMed]
13. Robel, I.; Subramanian, V.; Kuno, M.; Kamat, P.V. Quantum dot solar cells. Harvesting light energy with CdSe nanocrystals molecularly linked to mesoscopic TiO2 films. *J. Am. Chem. Soc.* **2006**, *128*, 2385–2393. [CrossRef] [PubMed]
14. Cooney, R.R.; Sewall, S.L.; Sagar, D.M.; Kambhampati, P. Gain Control in Semiconductor Quantum Dots via State-Resolved Optical Pumping. *Phys. Rev. Lett.* **2009**, *102*, 127404. [CrossRef] [PubMed]
15. Wang, Y.; Yu, D.; Wang, Z.; Li, X.; Chen, X.; Nalla, V.; Zeng, H.; Sun, H. Solution-Grown CsPbBr3/Cs4PbBr6 Perovskite Nanocomposites: Toward Temperature-Insensitive Optical Gain. *Small* **2017**, *13*, 1587.

16. Park, Y.-S.; Roh, J.; Diroll, B.T.; Schaller, R.D.; Klimov, V.I. Colloidal quantum dot lasers. *Nat. Rev. Mater.* **2021**, *6*, 382–401. [CrossRef]

17. Taghipour, N.; Dalmases, M.; Whitworth, G.L.; Dosil, M.; Othonos, A.; Christodoulou, S.; Liga, S.M.; Konstantatos, G. Colloidal Quantum Dot Infrared Lasers Featuring Sub-Single-Exciton Threshold and Very High Gain. *Adv. Mater.* **2023**, *35*, 2207678. [CrossRef]

18. Chen, O.; Riedemann, L.; Etoc, F.; Herrmann, H.; Coppey, M.; Barch, M.; Farrar, C.T.; Zhao, J.; Bruns, O.T.; Wei, H.; et al. Magneto-fluorescent core-shell supernanoparticles. *Nat. Commun.* **2014**, *5*, 5093. [CrossRef]

19. Wu, C.; Lu, Z.; Li, Z.; Yin, Y. Assembly of Colloidal Nanoparticles into Hollow Superstructures by Controlling Phase Separation in Emulsion Droplets. *Small Struct.* **2021**, *2*, 2100005. [CrossRef]

20. Kim, K.-H.; Dannenberg, P.H.; Yan, H.; Cho, S.; Yun, S.-H. Compact Quantum-Dot Microbeads with Sub-Nanometer Emission Linewidth. *Adv. Funct. Mater.* **2021**, *31*, 2103413. [CrossRef]

21. He, X.; Jia, K.; Bai, Y.; Chen, Z.; Liu, Y.; Huang, Y.; Liu, X. Quantum dots encoded white-emitting polymeric superparticles for simultaneous detection of multiple heavy metal ions. *J. Hazard. Mater.* **2021**, *405*, 124263. [CrossRef] [PubMed]

22. Lee, T.; Ohshiro, K.; Watanabe, T.; Hyeon-Deuk, K.; Kim, D. Temperature-Dependent Exciton Dynamics in CdTe Quantum Dot Superlattices Fabricated via Layer-by-Layer Assembly. *Adv. Opt. Mater.* **2022**, *10*, 2102781. [CrossRef]

23. Lan, X.; Chen, M.; Hudson, M.H.; Kamysbayev, V.; Wang, Y.; Guyot-Sionnest, P.; Talapin, D.V. Quantum dot solids showing state-resolved band-like transport. *Nat. Mater.* **2020**, *19*, 323–329. [CrossRef] [PubMed]

24. Crisp, R.W.; Schrauben, J.N.; Beard, M.C.; Luther, J.M.; Johnson, J.C. Coherent Exciton Delocalization in Strongly Coupled Quantum Dot Arrays. *Nano Lett.* **2013**, *13*, 4862–4869. [CrossRef]

25. Hou, K.; Han, J.; Tang, Z. Formation of Supraparticles and Their Application in Catalysis. *ACS Mater. Lett.* **2020**, *2*, 95–106. [CrossRef]

26. Wang, B.; Li, R.; Guo, G.; Xia, Y. Janus and core@shell gold nanorod@Cu2-xS supraparticles: Reactive site regulation fabrication, optical/catalytic synergetic effects and enhanced photothermal efficiency/photostability. *Chem. Commun.* **2020**, *56*, 8996–8999. [CrossRef]

27. Lin, C.H.; Lafalce, E.; Jung, J.; Smith, M.J.; Malak, S.T.; Aryal, S.; Yoon, Y.J.; Zhai, Y.; Lin, Z.; Vardeny, Z.V.; et al. Core/Alloyed-Shell Quantum Dot Robust Solid Films with High Optical Gains. *ACS Photonics* **2016**, *3*, 647–658. [CrossRef]

28. Gur, I.; Fromer, N.A.; Geier, M.L.; Alivisatos, A.P. Air-stable all-inorganic nanocrystal solar cells processed from solution. *Science* **2005**, *310*, 462–465. [CrossRef]

29. Yao, C.; Wang, P.; Li, X.; Hu, X.; Hou, J.; Wang, L.; Zhang, F. Near-Infrared-Triggered Azobenzene-Liposome/Upconversion Nanoparticle Hybrid Vesicles for Remotely Controlled Drug Delivery to Overcome Cancer Multidrug Resistance. *Adv. Mater.* **2016**, *28*, 9341–9348. [CrossRef]

30. Klimov, V.I.; Mikhailovsky, A.A.; McBranch, D.W.; Leatherdale, C.A.; Bawendi, M.G. Quantization of multiparticle Auger rates in semiconductor quantum dots. *Science* **2000**, *287*, 1011–1013. [CrossRef]

31. Talapin, D.V.; Lee, J.-S.; Kovalenko, M.V.; Shevchenko, E.V. Prospects of Colloidal Nanocrystals for Electronic and Optoelectronic Applications. *Chem. Rev.* **2010**, *110*, 389–458. [CrossRef] [PubMed]

32. Zhao, Y.; Shang, L.; Cheng, Y.; Gu, Z. Spherical Colloidal Photonic Crystals. *Acc. Chem. Res.* **2014**, *47*, 3632–3642. [CrossRef] [PubMed]

33. Park, J.-G.; Kim, S.-H.; Magkiriadou, S.; Choi, T.M.; Kim, Y.-S.; Manoharan, V.N. Full-Spectrum Photonic Pigments with Non-iridescent Structural Colors through Colloidal Assembly. *Angew. Chem. Int. Ed.* **2014**, *53*, 2899–2903. [CrossRef] [PubMed]

34. Vogel, N.; Utech, S.; England, G.T.; Shirman, T.; Phillips, K.R.; Koay, N.; Burgess, I.B.; Kolle, M.; Weitz, D.A.; Aizenberg, J. Color from hierarchy: Diverse optical properties of micron-sized spherical colloidal assemblies. *Proc. Natl. Acad. Sci. USA* **2015**, *112*, 10845–10850. [CrossRef]

35. Marino, E.; Sciortino, A.; Berkhout, A.; MacArthur, K.E.; Heggen, M.; Gregorkiewicz, T.; Kodger, T.E.; Capretti, A.; Murray, C.B.; Koenderink, A.F.; et al. Simultaneous Photonic and Excitonic Coupling in Spherical Quantum Dot Supercrystals. *ACS Nano* **2020**, *14*, 13806–13815. [CrossRef]

36. Chen, X.; Fu, Z.; Gong, Q.; Wang, J. Quantum entanglement on photonic chips: A review. *Adv. Photonics* **2021**, *3*, 064002. [CrossRef]

37. Jiang, B.; Zhu, S.; Ren, L.; Shi, L.; Zhang, X. Simultaneous ultraviolet, visible, and near-infrared continuous-wave lasing in a rare-earth-doped microcavity. *Adv. Photonics* **2022**, *4*, 046003. [CrossRef]

38. Shuklov, I.A.; Toknova, V.F.; Lizunova, A.A.; Razumov, V.F. Controlled aging of PbS colloidal quantum dots under mild conditions. *Mater. Today Chem.* **2020**, *18*, 100357. [CrossRef]

39. Wu, J.; Su, R.; Fieramosca, A.; Ghosh, S.; Zhao, J.; Liew, T.C.H.; Xiong, Q. Perovskite polariton parametric oscillator. *Adv. Photonics* **2021**, *3*, 055003. [CrossRef]

40. Bai, F.; Wang, D.; Huo, Z.; Chen, W.; Liu, L.; Liang, X.; Chen, C.; Wang, X.; Peng, Q.; Li, Y. A versatile bottom-up assembly approach to colloidal spheres from nanocrystals. *Angew. Chem. Int. Ed.* **2007**, *46*, 6650–6653. [CrossRef]

41. De Nijs, B.; Dussi, S.; Smallenburg, F.; Meeldijk, J.D.; Groenendijk, D.J.; Filion, L.; Imhof, A.; van Blaaderen, A.; Dijkstra, M. Entropy-driven formation of large icosahedral colloidal clusters by spherical confinement. *Nat. Mater.* **2015**, *14*, 56–60. [CrossRef] [PubMed]

42. Lacava, J.; Ouali, A.-A.; Raillard, B.; Kraus, T. On the behaviour of nanoparticles in oil-in-water emulsions with different surfactants. *Soft Matter* **2014**, *10*, 1696–1704. [CrossRef] [PubMed]

43. Plunkett, A.; Eldridge, C.; Schneider, G.A.; Domenech, B. Controlling the Large-Scale Fabrication of Supraparticles. *J. Phys. Chem. B* **2020**, *124*, 11263–11272. [CrossRef] [PubMed]

44. Koshkina, O.; Raju, L.T.; Kaltbeitzel, A.; Riedinger, A.; Lohse, D.; Zhang, X.; Landfester, K. Surface Properties of Colloidal Particles Affect Colloidal Self-Assembly in Evaporating Self-Lubricating Ternary Droplets. *ACS Appl. Mater. Interfaces* **2022**, *14*, 2275–2290. [CrossRef]

45. Marino, E.; Kodger, T.E.; Wegdam, G.H.; Schall, P. Revealing Driving Forces in Quantum Dot Supercrystal Assembly. *Adv. Mater.* **2018**, *30*, 1803433. [CrossRef]

46. Montanarella, F.; Geuchies, J.J.; Dasgupta, T.; Prins, P.T.; van Overbeek, C.; Dattani, R.; Baesjou, P.; Dijkstra, M.; Petukhov, A.V.; van Blaaderen, A.; et al. Crystallization of Nanocrystals in Spherical Confinement Probed by in Situ X-ray Scattering. *Nano Lett.* **2018**, *18*, 3675–3681. [CrossRef]

47. Schmitt, J.; Hajiw, S.; Lecchi, A.; Degrouard, J.; Salonen, A.; Imperor-Clerc, M.; Pansu, B. Formation of Superlattices of Gold Nanoparticles Using Ostwald Ripening in Emulsions: Transition from fcc to bcc Structure. *J. Phys. Chem. B* **2016**, *120*, 5759–5766. [CrossRef]

48. Marino, E.; Keller, A.W.; An, D.; van Dongen, S.; Kodger, T.E.; MacArthur, K.E.; Heggen, M.; Kagan, C.R.; Murray, C.B.; Schall, P. Favoring the Growth of High-Quality, Three-Dimensional Supercrystals of Nanocrystals. *J. Phys. Chem. C* **2020**, *124*, 11256–11264. [CrossRef]

49. Wang, D.; van der Wee, E.B.; Zanaga, D.; Altantzis, T.; Wu, Y.; Dasgupta, T.; Dijkstra, M.; Murray, C.B.; Bals, S.; van Blaaderen, A. Quantitative 3D real-space analysis of Laves phase supraparticles. *Nat. Commun.* **2021**, *12*, 3980. [CrossRef]

50. Montanarella, F.; Altantzis, T.; Zanaga, D.; Rabouw, F.T.; Bals, S.; Baesjou, P.; Vanmaekelbergh, D.; van Blaaderen, A. Composite Supraparticles with Tunable Light Emission. *ACS Nano* **2017**, *11*, 9136–9142. [CrossRef]

51. Zou, H.; Wang, D.; Gong, B.; Liu, Y. Preparation of CdTe superparticles for white light-emitting diodes without Forster resonance energy transfer. *RSC Adv.* **2019**, *9*, 30797–30802. [CrossRef] [PubMed]

52. Vanmaekelbergh, D.; van Vugt, L.K.; Bakker, H.E.; Rabouw, F.T.; de Nijs, B.; van Dijk-Moes, R.J.A.; van Huis, M.A.; Baesjou, P.J.; van Blaaderen, A. Shape-Dependent Multiexciton Emission and Whispering Gallery Modes in Supraparticles of CdSe/Multishell Quantum Dots. *ACS Nano* **2015**, *9*, 3942–3950. [CrossRef] [PubMed]

53. Montanarella, F.; Urbonas, D.; Chadwick, L.; Moerman, P.G.; Baesjou, P.J.; Mahrt, R.F.; van Blaaderen, A.; Stoferle, T.; Vanmaekelbergh, D. Lasing Supraparticles Self-Assembled from Nanocrystals. *ACS Nano* **2018**, *12*, 12788–12794. [CrossRef] [PubMed]

54. Neuhaus, S.J.; Marino, E.; Murray, C.B.; Kagan, C.R. Frequency Stabilization and Optically Tunable Lasing in Colloidal Quantum Dot Superparticles. *Nano Lett.* **2023**, *23*, 645–651. [CrossRef] [PubMed]

55. Chang, H.; Zhong, Y.; Dong, H.; Wang, Z.; Xie, W.; Pan, A.; Zhang, L. Ultrastable low-cost colloidal quantum dot microlasers of operative temperature up to 450 K. *Light Sci. Appl.* **2021**, *10*, 60. [CrossRef]

56. Gao, Z.; Zhang, W.; Yan, Y.; Yi, J.; Dong, H.; Wang, K.; Yao, J.; Zhao, Y.S. Proton-Controlled Organic Microlaser Switch. *ACS Nano* **2018**, *12*, 5734–5740. [CrossRef]

57. Blondot, V.; Bogicevic, A.; Coste, A.; Arnold, C.; Buil, S.; Quelin, X.; Pons, T.; Lequeux, N.; Hermier, J.-P. Fluorescence properties of self assembled colloidal supraparticles from CdSe/CdS/ZnS nanocrystals. *New J. Phys.* **2020**, *22*, 113026. [CrossRef]

58. Montanarella, F.; Biondi, M.; Hinterding, S.M.; Vanmaekelbergh, D.; Rabouw, F.T. Reversible Charge-Carrier Trapping Slows Forster Energy Transfer in CdSe/CdS Quantum-Dot Solids. *Nano Lett.* **2018**, *18*, 5867–5874. [CrossRef]

59. Kister, T.; Mravlak, M.; Schilling, T.; Kraus, T. Pressure-controlled formation of crystalline, Janus, and core-shell supraparticles. *Nanoscale* **2016**, *8*, 13377–13384. [CrossRef]

60. Wang, J.; Mbah, C.F.; Przybilla, T.; Zubiri, B.A.; Spiecker, E.; Engel, M.; Vogel, N. Magic number colloidal clusters as minimum free energy structures. *Nat. Commun.* **2018**, *9*, 5259. [CrossRef]

61. Kim, C.; Jung, K.; Yu, J.W.; Park, S.; Kim, S.-H.; Lee, W.B.; Hwang, H.; Manoharan, V.N.; Moon, J.H. Controlled Assembly of Icosahedral Colloidal Clusters for Structural Coloration. *Chem. Mater.* **2020**, *32*, 9704–9712. [CrossRef]

62. Chou, K.F.; Dennis, A.M. Forster Resonance Energy Transfer between Quantum Dot Donors and Quantum Dot Acceptors. *Sensors* **2015**, *15*, 13288–13325. [CrossRef] [PubMed]

63. Clapp, A.R.; Medintz, I.L.; Mauro, J.M.; Fisher, B.R.; Bawendi, M.G.; Mattoussi, H. Fluorescence resonance energy transfer between quantum dot donors and dye-labeled protein acceptors. *J. Am. Chem. Soc.* **2004**, *126*, 301–310. [CrossRef] [PubMed]

64. Hou, X.; Kang, J.; Qin, H.; Chen, X.; Ma, J.; Zhou, J.; Chen, L.; Wang, L.; Wang, L.-W.; Peng, X. Engineering Auger recombination in colloidal quantum dots via dielectric screening. *Nat. Commun.* **2019**, *10*, 1750. [CrossRef]

65. Vaxenburg, R.; Rodina, A.; Shabaev, A.; Lifshitz, E.; Efros, A.L. Nonradiative Auger Recombination in Semiconductor Nanocrystals. *Nano Lett.* **2015**, *15*, 2092–2098. [CrossRef]

66. Javaux, C.; Mahler, B.; Dubertret, B.; Shabaev, A.; Rodina, A.V.; Efros, A.L.; Yakovlev, D.R.; Liu, F.; Bayer, M.; Camps, G.; et al. Thermal activation of non-radiative Auger recombination in charged colloidal nanocrystals. *Nat. Nanotechnol.* **2013**, *8*, 206–212. [CrossRef]

67. Algar, W.R.; Kim, H.; Medintz, I.L.; Hildebrandt, N. Emerging non-traditional Forster resonance energy transfer configurations with semiconductor quantum dots: Investigations and applications. *Coord. Chem. Rev.* **2014**, *263*, 65–85. [CrossRef]